Effect of valence fluctuations in A sites on the transport properties of $La_{1-x}R_xMnO_3$ (R = Ce, Pr)

1999 J. Phys.: Condens. Matter 11 8537

(http://iopscience.iop.org/0953-8984/11/43/317)

J. Phys.: Condens. Matter **11** (1999) 8537–8546. Printed in the UK PII: S0953-8984(99)05036-5

Effect of valence fluctuations in A sites on the transport properties of $La_{1-x}R_xMnO_3$ (R = Ce, Pr)

John Philip and T R N Kutty
Materials Research Centre, Indian Institute of Science, Bangalore 560 012, India

Received 8 June 1999, in final form 24 August 1999

Abstract. $La_{1-x}R_xMnO_3$ (R = Ce or Pr) exhibit valence fluctuations (R^{3+} and R^{4+}) in the A sublattice of the ABO_3 perovskite structure. They also display a metal–insulator (M–I) transition and magnetoresistance effect even without the substitution of divalent cations. In $La_{1-x}Ce_xMnO_3$, as Ce concentration increases ($x = 0.05$ to 0.6), the magnitude of resistivity decreases and the magnetic transition temperature, T_c, shifts towards higher temperature. The change in transport properties is attributed to the increase in Mn^{3+}–Mn^{4+} pairs. The electronic and magnetic phase diagram is obtained for $La_{1-x}Ce_xMnO_3$ from the resistivity and dc susceptibility measurements over a broad range of temperature and concentrations. The thermopower and magnetoresistance are also measured for $La_{1-x}Ce_xMnO_3$ for two x values ($x = 0.3$ and 0.6). The high temperature thermopower data fit to an adiabatic small polaron hopping mechanism.

1. Introduction

The electronic and magnetic properties of perovskite manganites depend on several correlated factors, including the mixed valence of Mn, double exchange, Jahn–Teller distortion and A site ionic radius (lattice coupling) [1–3]. In lanthanum calcium manganites, since La and Ca have fixed valence, there is no valence fluctuation in the A sublattice of the ABO_3 perovskite structure. Substitution of Ca introduces valence fluctuations in the B site, thereby producing holes. In the case of Ce and Pr substituted manganites ($La_{1-x}Ce_xMnO_3$ and $La_{1-x}Pr_xMnO_3$), the rare-earth elements in the A site have multiple valence states and these can further increase the charge disorder in the Mn (Mn^{2+}, Mn^{3+} and Mn^{4+}) site. There are a few studies about these compounds related to the colossal magnetoresistance (CMR) property, but none of the papers have taken the multiple valence states of Ce or Pr into account [4–6]. Ce and Pr in many of the oxides have stable valence of +4. Here we report the effect of valence fluctuations in the A site on the transport properties of $La_{1-x}R_xMnO_3$ (R = Ce, Pr). A detailed investigation is carried out on the $La_{1-x}Ce_xMnO_3$ system and its phase diagram is drawn. In order to understand the effect of charge disorder in the A site, we have substituted the La site with Ce or Pr without the addition of divalent cations. Thus the multiple oxidation states exhibited by the Mn ions can be attributed to the charge disorder in the Ce/Pr sites. Normally in manganite perovskites, divalent cation substitution introduces holes and modifies the magnetic as well as electrical transport properties. Addition of Ca, Sr or Ba in $LaMnO_3$ (moderate doping) changes the ground state from an anti-ferromagnetic insulator to ferromagnetic metal in association with large CMR near the magnetic transition temperature (T_c). However in the case of $La_{1-x}R_xMnO_3$ ($x = 0.2$–0.8), even without the substitution of divalent cations, they exhibit a paramagnetic insulator to ferromagnetic metal transition and the magnetoresistance (MR)

0953-8984/99/438537+10$30.00

effect. Various La–Ce/Pr–manganite compositions have been prepared and their structural, transport and magnetic properties were studied.

2. Experiment

$La_{1-x}(Ce/Pr)_xMnO_3$ compounds were prepared through a wet-chemical method involving a redox reaction. MnO_2 was precipitated from the reaction of $KMnO_4$ with $MnSO_4 \cdot H_2O$ salts in acidic medium in the presence of other metal ions like La, Ce or Pr, Ca, which were then precipitated completely by raising the pH to 7. The precipitate was filtered and washed with deionized water and decomposed at 1123 K obtaining phase-pure lanthanum–cerium/praseodymium manganites ($La_{1-x}(Ce/Pr)_xMnO_3$). The details of the method were given in [7]. These compounds were pressed into discs and sintered in air for 5 h at 1673 K and used for electrical and magnetic measurements. X-ray diffraction (XRD) patterns were obtained using a Scintag (USA) diffractometer. The ferromagnetic transition temperatures were obtained from the susceptibility measurements using the Gouy method [8]. Electrical resistivity, $\rho(T)$, was measured using the four-probe dc technique. The concentration of Mn^{4+} was determined by iodometric titrations using sodium thiosulphate [9]. The thermopower measurements were carried out using a dc technique by supplying heat at one end of a sintered bar and measuring the resulting thermo-emf and the differential temperature [10].

3. Results and discussion

3.1. XRD studies

X-ray diffraction patterns of various La–Ce/Pr–manganite compositions sintered at 1673 K are shown in figures 1 and 2. All the compositions exhibit single phasic character. Ce substituted compositions display an orthorhombic crystal symmetry, whereas the Pr samples crystallize in tetragonal symmetry. The unit cell volume decreases with the Ce or Pr content. Different compositions and their crystal symmetries are presented in table 1. Under identical conditions, calcium substituted $LaMnO_3$ exhibits cubic symmetry. Deviations from the cubic symmetry in $La_{1-x}R_xMnO_3$ are due to the valence fluctuations and size differences in the A sublattice ions (R^{3+}, R^{4+} and La^{3+}).

Table 1. Crystal systems and lattice parameters of $La_{1-x}(Ce/Pr)_xMnO_3$ manganites.

La–(Ce/Pr) compositions	Crystal symmetry	a (Å)	b (Å)	c (Å)	V (Å^3)
$La_{0.95}Ce_{0.05}MnO_3$	Orthorhombic	5.543	5.594	7.805	242.01
$La_{0.7}Ce_{0.3}MnO_3$	Orthorhombic	5.403	5.519	7.759	231.36
$La_{0.4}Ce_{0.6}MnO_3$	Orthorhombic	5.400	5.500	7.765	230.62
$La_{0.2}Ce_{0.8}MnO_3$	Orthorhombic	5.400	5.450	7.785	229.11
$La_{0.8}Pr_{0.2}MnO_3$	Tetragonal	5.490	5.490	7.765	234.07
$La_{0.4}Pr_{0.6}MnO_3$	Tetragonal	5.470	5.470	7.750	231.88

Iodometric titrations were carried out to estimate the oxidation states of Ce, Pr and Mn ions. Ce and Pr exhibit two different valence states and Mn exhibits three possible valence states. The distributions of oxidation states for various compositions are given in table 2. All the compositions show the presence of both R^{3+} and R^{4+} in the A site and Mn^{2+}, Mn^{3+} and Mn^{4+} in the Mn site. The R^{4+} ions may not be in the 12-fold coordination in the A site, as in the case of La^{3+}; however, they may locally distort the perovskite structure to be in higher coordination without disturbing the large-scale perovskite structure.

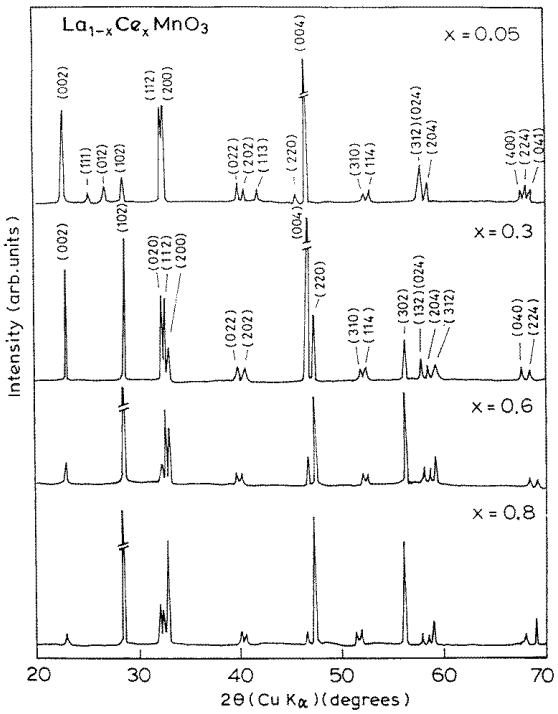

Figure 1. X-ray diffraction traces of $La_{1-x}Ce_xMnO_3$ ($x = 0.05$, 0.3, 0.6 and 0.8).

Table 2. Concentration of oxidation states of Ce/Pr, Mn ions and the δ values in different La–Ce/Pr manganite compositions.

La–Ce compositions	Ce^{4+}/Pr^{4+}	Mn^{4+}	Mn^{2+}	Excess oxygen content (δ)
$La_{0.95}Ce_{0.05}MnO_{3+\delta}$	0.05	0.22	0.02	0.125
$La_{0.7}Ce_{0.3}MnO_{3+\delta}$	0.25	0.35	0.05	0.275
$La_{0.4}Ce_{0.6}MnO_{3+\delta}$	0.56	0.40	0.10	0.43
$La_{0.1}Ce_{0.6}Ca_{0.3}MnO_{3+\delta}$	0.56	0.375	0.115	0.260
$La_{0.4}Pr_{0.6}MnO_{3+\delta}$	0.5	0.33	0.27	0.28
$La_{0.8}Pr_{0.2}MnO_{3+\delta}$	0.16	0.11	0.09	0.09

3.2. Resistivity

Figure 3(a) presents the resistivity, $\rho(T)$, versus temperature (T) plots of $La_{1-x}Ce_xMnO_3$ for various x values, sintered at 1673 K for 5 h in air. Studies are mainly carried out on the as-sintered sample to understand the effect of multiple valence states (Mn^{2+}, Mn^{3+} and Mn^{4+}) introduced in the Mn sublattice by the presence of Ce^{4+} in the A sublattice. $La_{0.95}Ce_{0.05}MnO_3$ exhibits a completely insulating behaviour in the temperature range that is used for measurement. There is a transition from paramagnetic insulating to ferromagnetic insulating state around 245 K. The magnetic transition temperature, T_c, is obtained from the susceptibility data in figure 4(c). Parent, stoichiometric $LaMnO_3$ is a well known antiferromagnetic insulator. Ritter *et al* [11] have shown that as the oxygen nonstoichiometry increases, $LaMnO_{3+\delta}$ ($\delta \geqslant 0.1$) behaves as a ferromagnetic insulator. Similar behaviour is

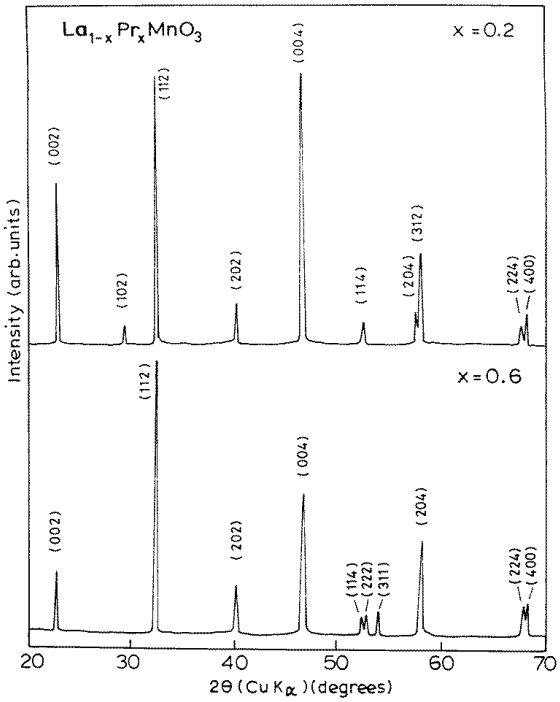

Figure 2. X-ray diffraction traces of $La_{1-x}Pr_xMnO_3$ (x=0.2 and 0.6).

observed in $La_{0.95}Ce_{0.05}MnO_{3+\delta}$ ($\delta = 0.125$) and it is interesting to note that the as-sintered sample exhibits this δ value. $La_{1-x}Ce_xMnO_3$ exhibits an insulating behaviour for $x \leqslant 0.2$. For $x > 0.2$, there is a changeover from insulating to metallic phase associated with a magnetic transition from para- to ferromagnetic phase as indicated by the susceptibility data in figure 4. La–Ce manganites ($x = 0.3$ to 0.8) display similar $\rho(T)$ characteristics as in the case of Ca ($x = 0.1$–0.4) substituted $LaMnO_3$ [12]; however $La_{1-x}Ce_xMnO_3$ phases exhibit large resistivity values (10–10^4 Ω cm). The magnitude of resistivity decreases (from $x = 0.05$ to $x = 0.6$) and T_c shifts towards room temperature as the Ce content increases. Gebhardt *et al* [6] have shown that $\rho(T)$ increases with the Ce content ($x = 0.2$–0.4). They attribute this increase in $\rho(T)$ to the increasing concentration of the secondary phase (MnO_2) in their samples. We do not observe any secondary phases in our samples. Mandal and Das [4] have shown that $La_{0.7}Ce_{0.3}MnO_3$ exhibits low resistivity (1–6 Ω cm) in comparison to our as-sintered sample. The difference in magnitude in $\rho(T)$ arises due to the processing conditions. Mandal and Das have sintered their sample at 1373 K for 96 h with intermediate grindings. Sintering at lower temperatures (∼1373 K) for extended duration increases the δ value and thereby decreases $\rho(T)$, but these samples lack high density exhibiting high porosity. Figure 5 displays the $\rho(T)$ characteristics of $La_{1-x}Pr_xMnO_3$ for two x values. They also exhibit similar behaviour to that of Ce-substituted samples; however there is no discernable change in the M–I transition temperature with Pr content as in the case of Ce compositions. Figure 3(b) shows the modified $\rho(T)$ characteristics of $La_{0.7}Ce_{0.3}MnO_3$ after annealing in oxygen at 1273 K. The magnitude of $\rho(T)$ reduces from 700 to 9 Ω cm and shifts the T_c to higher temperatures.

In the results presented in figure 3(a), $\rho(T)$ decreases with increase of Ce content (from $x = 0.05$ to 0.6). The decrease can be accounted for by considering the valence fluctuations in the Mn site arising due to the fluctuation in the Ce sites. The data in table 2 indicate that with

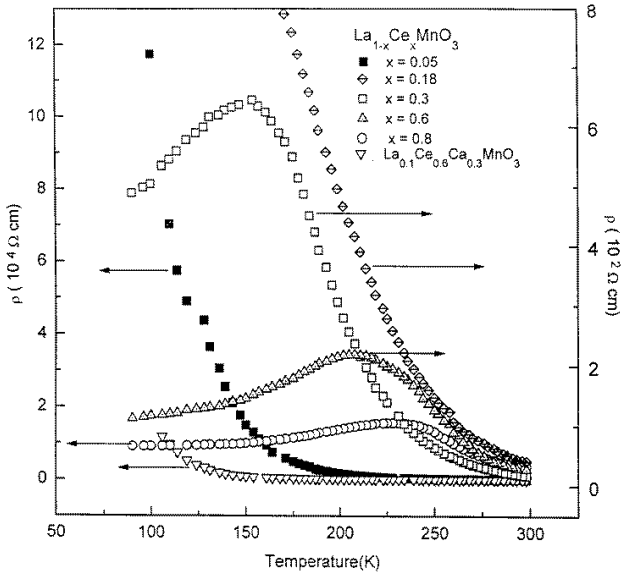

(a)

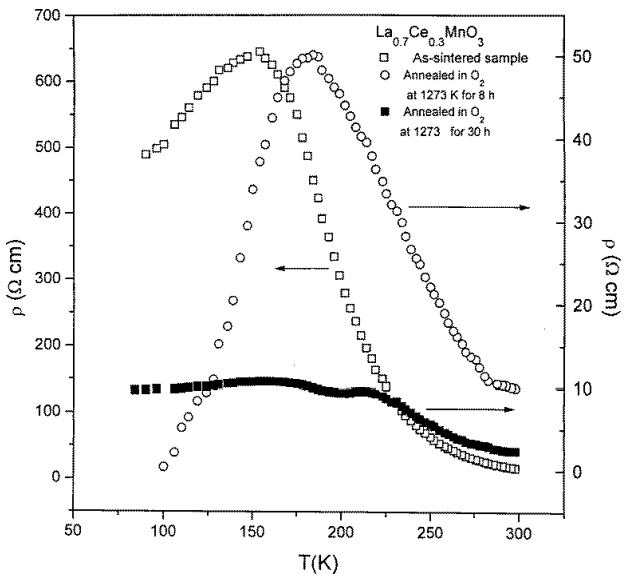

(b)

Figure 3. (a) Resistivity, $\rho(T)$, versus temperature plots of $La_{1-x}Ce_xMnO_3$ for various x values ($x = 0.05, 0.18, 0.3, 0.6, 0.8$ and $La_{0.1}Ce_{0.6}Ca_{0.3}MnO_3$). (b) Resistivity, $\rho(T)$, versus temperature plots of $La_{0.7}Ce_{0.3}MnO_3$ sample after annealing in oxygen at 1273 K.

the Ce content, the concentration of both holes and Mn^{2+} increases. High concentration of Ce^{4+} in the A site can lead to large oxygen excess ($La_{1-x}Ce_xMnO_{3+\delta}$) conditions in all the La–Ce compositions. The sample with $x = 0.6$ shows a large δ value of 0.43. In such oxygen excess conditions, Mn ions can stabilize in +4 or +3 oxidation states in addition to the presence of

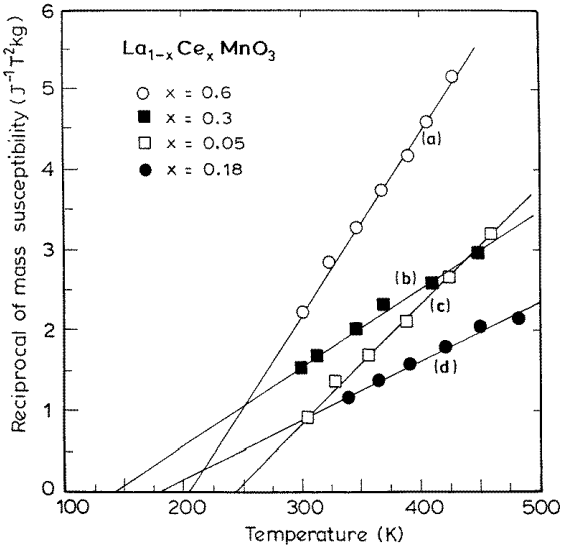

Figure 4. Reciprocal of mass susceptibility is plotted against T for $La_{1-x}Ce_xMnO_3$: (a) $x = 0.6$; (b) $x = 0.3$; (c) $x = 0.05$; (d) $x = 0.18$.

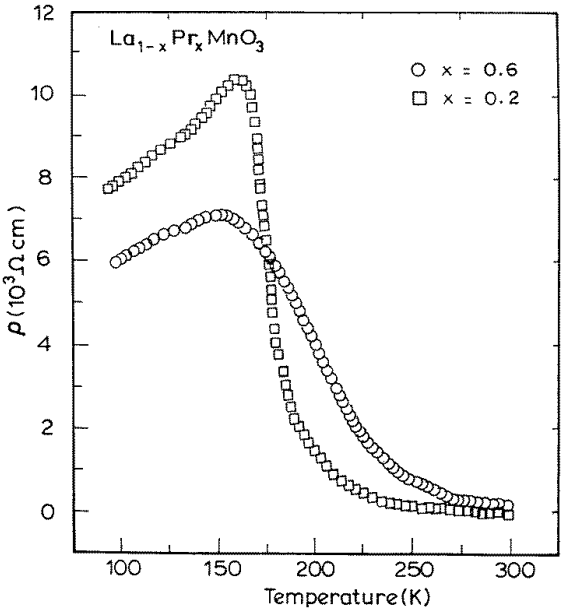

Figure 5. Resistivity versus temperature plots of $La_{1-x}Pr_xMnO_3$ ($x = 0.2$ and 0.6).

Mn^{2+} ions depending upon the extent of nonstoichiometry. Thus, Mn ions are present in three different oxidation states and, in each La–Ce compositions, Mn^{3+}–Mn^{4+} pairs increase with Ce ($x = 0.05$–0.6) content over Mn^{2+}–Mn^{3+} pairs. Therefore double exchange (Mn^{3+}–O–Mn^{4+}) dominates over other super-exchange (Mn^{3+}–O–Mn^{3+}, Mn^{2+}–O–Mn^{3+}) mechanisms resulting in M–I transition and shift of T_c to higher temperatures. In the case of La–Pr manganites,

there are almost equal numbers of Mn^{3+}–Mn^{4+} and Mn^{2+}–Mn^{3+} pairs. Thus there will be competition between double exchange and super-exchange resulting in high resistivity [13] and the shift in ferromagnetic transition temperature to higher temperature with Pr addition is suppressed. The same mechanism can explain the high $\rho(T)$ exhibited by $La_{0.2}Ce_{0.8}MnO_3$. The electron hopping between Mn^{2+}/Mn^{3+} states is rarely observed, relative to the more frequent Mn^{4+}/Mn^{3+} hole hopping [14]. This is because the characteristic small polaron energy is determined, in part, by the difference in bond lengths between initial and final configuration oxidation states; 50% larger ionic size difference between Mn^{2+}/Mn^{3+} ions relative to that of Mn^{3+}/Mn^{4+} indicates that Mn^{2+}/Mn^{3+} electron hopping will occur; it will do so at a considerably lower rate than that of hole hopping between Mn^{4+}/Mn^{3+} states. Hence, Mn^{2+} sites can be assumed to act as blocking sites for polaron transport. In figure 3(a), the insulating $\rho(T)$ behaviour of $La_{0.1}Ce_{0.6}Ca_{0.3}MnO_3$ is shown. Comparing the electronic and magnetic properties of $La_{0.1}Ce_{0.6}Ca_{0.3}MnO_3$ with $La_{0.4}Ce_{0.6}MnO_3$, addition of 30% Ca to the latter completely destroys the ferromagnetic metallic state and displays a ferromagnetic insulating state. This may be due to the interaction between the electrons and holes present in the system, so that there is an annihilation of charge carriers in addition to the A site cation size effect.

The electronic and magnetic phase diagram of $La_{1-x}Ce_xMnO_3$ is given in figure 6. The phase diagram is obtained from the as-sintered samples. For all $x \leqslant 0.2$, the material is ferromagnetic at low temperatures and displays insulating behaviour ($d\rho/dT < 0$) for the complete range of temperature measured. For $x > 0.2$, the materials displayed a drop in resistivity into the low temperature metallic state and the peak in $\rho(T)$ is strongly correlated with the ferromagnetic transition. The resistivity range in the metallic regime is several orders of magnitude higher than the Mott maximum metallic resistivity. In clean metallic manganites, the calculated maximum metallic resistivity is about 1–2 mΩ cm [15]. Ca substituted $LaMnO_3$ ($La_{1-x}Ca_xMnO_3$) exhibits a charge ordered antiferromagnetic insulating state for $x \geqslant 0.5$ and such behaviour is not observed with the Ce substitution.

Figure 7 displays the $\log(\rho(T)$ versus $1/T$ plots of the two La–Ce compositions ($x = 0.3$ and 0.6). The high temperature region can be fitted with the expression for the adiabatic small polaron conduction mechanism:

$$\rho(T) = \rho_0 T \exp\left(\frac{E_a}{k_B T}\right) \tag{1}$$

where E_a is the activation energy of hopping and k_B is Boltzmann's constant. Activation energy E_a values are calculated from the slope of the fitted straight line and presented in table 3.

Table 3. Activation energies from resistivity and thermopower plots for $La_{1-x}Ce_xMnO_3$.

La–Ce compositions	E_a (meV)	E_s (meV)
$La_{0.7}Ce_{0.3}MnO_3$	162	106
$La_{0.4}Ce_{0.6}MnO_3$	159	14

3.3. Thermopower

Figure 8 shows the thermopower, $S(T)$, plotted against $1/T$ for two Ce compositions. The value of S is positive in the measured temperature indicating a hole-like behaviour for the carriers. Similar thermopower behaviour was observed by Mandal and Das [4] for $La_{0.7}Ce_{0.3}MnO_3$. In these compounds $|S|$ values are large in comparison to Ca substituted

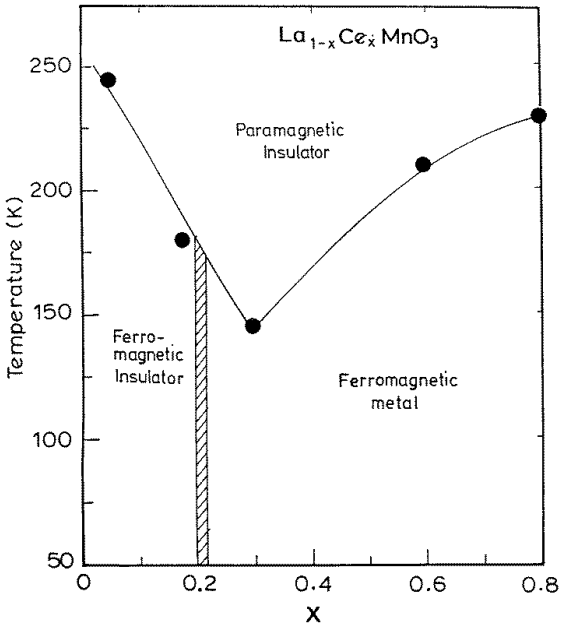

Figure 6. Electronic and magnetic phase diagram of $La_{1-x}Ce_xMnO_3$ (from the resistivity and susceptibility data).

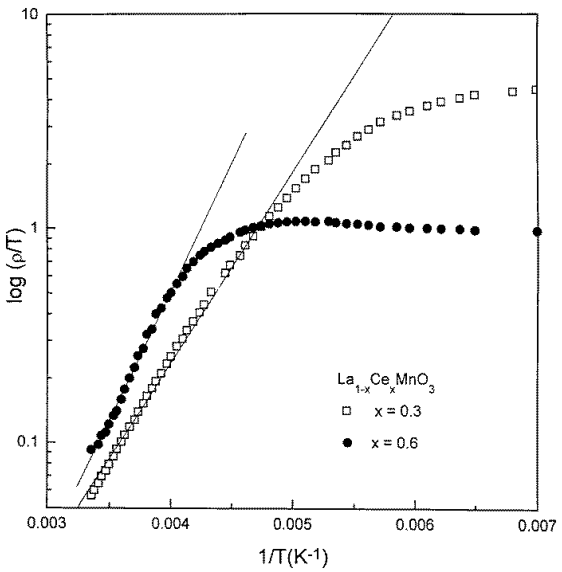

Figure 7. $\log(\rho/T)$ versus $1/T$ for $La_{1-x}Ce_xMnO_3$ ($x = 0.3$ and 0.6).

$LaMnO_3$ (∼0–60 μV K^{-1}). $|S|$ increases with decreasing T. At T slightly greater than T_c, it starts decreasing indicating a metal-like behaviour. Similar behaviour is observed in $La_{1-x}Ca_xMnO_{3+\delta}$ samples. In $La_{0.79}Ca_{0.21}MnO_{3+0.017}$, S peaks roughly 20 K above T_c [16]. For $T < T_c$, $|S|$ is almost constant, and in the high temperature regime ($T > T_c$), thermopower

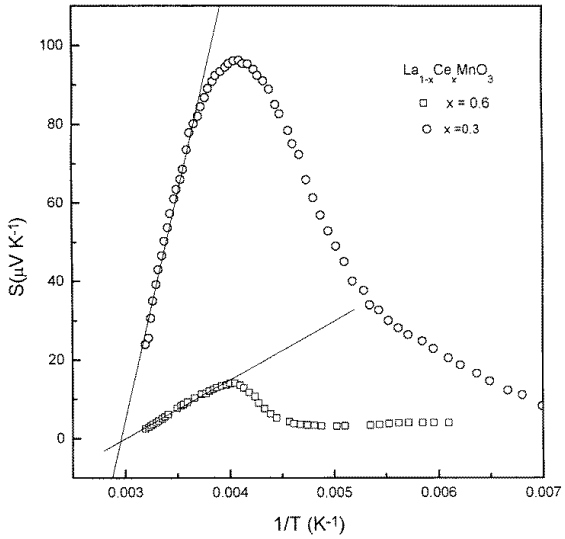

Figure 8. The temperature dependence of the thermopower of $La_{1-x}Ce_xMnO_3$ ($x = 0.3$ and 0.6).

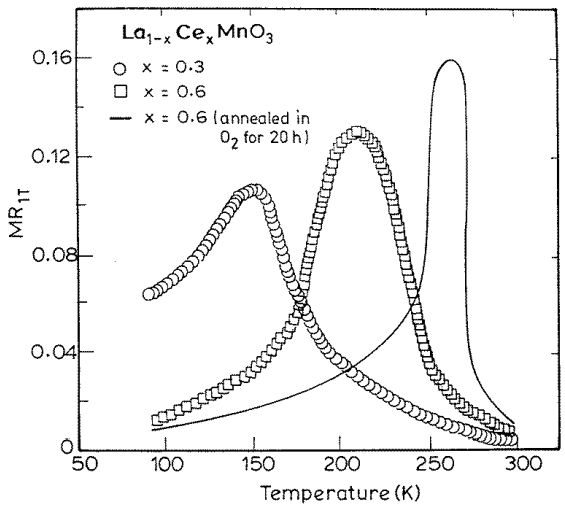

Figure 9. Magnetoresistance ($MR_H = (\rho(0) - \rho(H))/\rho(0)$) versus T plots for $La_{1-x}Ce_xMnO_3$ ($x = 0.3$, 0.6 and oxygen annealed (20 h) $x = 0.6$ sample).

satisfies the adiabatic small polaron hopping theory. According to this theory, thermopower can be expressed as

$$S(T) = \left(\frac{k_B}{e}\right)\left(\alpha + \frac{E_s}{k_B T}\right) \tag{2}$$

where E_s is the activation energy, e is the electronic charge and α is a sample-dependent constant. S versus $1/T$ curves fit well with the equation (2) in the high temperature regime and the E_s values are calculated from the slope. E_s values are presented in table 3 together with the activation energy values obtained from the resistivity plots ($\log(\rho(T)/T$ versus $1/T$).

The resistivity and thermopower show different values for the activation energy indicating that the charge transport is by hopping of charge carriers rather than semiconducting-like activated conduction.

3.4. Magnetoresistance

Figure 9 presents the magnetoresistance, defined as $MR_H = (\rho(0) - \rho(H))/\rho(0)$ versus temperature plots for $La_{0.7}Ce_{0.3}MnO_3$ and $La_{0.4}Ce_{0.6}MnO_3$. These compounds show a magnetoresistance of ∼10–15% at a magnetic field of 1 T. The MR curve of the oxygen annealed $La_{0.4}Ce_{0.6}MnO_3$ sample is very sharp and its peak value has shifted to higher temperature. Thus oxygen annealing increases the Mn^{3+}–Mn^{4+} pairs and thereby decreases the magnitude of the resistivity and shifts T_c to higher temperatures.

4. Conclusions

In summary, we have obtained the electronic and magnetic phase diagram of $La_{1-x}Ce_xMnO_3$. Ce/Pr exhibits multiple valence states (R^{3+}, R^{4+}) in the A sublattice and Mn^{2+}, Mn^{3+} and Mn^{4+} ions in the Mn sites. The presence of multiple valence states in A sites changes the resistivity characteristics. The change in $\rho(T)$ behaviour in $La_{1-x}R_xMnO_3$ may be due to the large charge disorder present in both the sublattices. The thermopower shows hole-like carrier behaviour and the high temperature thermopower data can fit into an adiabatic small polaron mechanism. Magnetoresistance is observed for the compositions exhibiting M–I transitions and MR maximizes near the transition temperature.

References

[1] Millis A J, Littlewood P B and Shraiman B I 1995 *Phys. Rev. Lett.* **74** 5144
[2] Fontcuberta J, Martinez B, Seffar A, Pinol S, Garcia-Munoz J L and Obradors X 1996 *Phys. Rev. Lett.* **76** 1122
[3] Hwang H Y, Cheong S W, Radaelli P G, Marezio M and Batlogg M 1995 *Phys. Rev. Lett.* **75** 914
[4] Mandal P and Das S 1997 *Phys. Rev.* B **56** 15 073
[5] Tokura Y, Tomioka Y, Kuwahara H, Asamitsu A, Moritomo Y and Kasai M 1996 *J. Appl. Phys.* **79** 5288
[6] Gebhardt J R, Roy S and Ali N S 1999 *J. Appl. Phys.* **85** 5390
[7] Philip J and Kutty T R N 1999 *Mater. Chem. Phys.* at press
Philip J and Kutty T R N 1999 *Mater. Lett.* **39** 311
[8] Crangle J 1977 *The Magnetic Properties of Solids* (London: Arnold) p 161
[9] Vogel I 1989 *Textbook of Quantitative Chemical Analysis* (Addison-Wesley–Longman) p 384
[10] Heikes R R and Ure R W Jr 1961 *Thermoelectricity: Science and Engineering* (New York: Interscience) p 285
[11] Ritter C, Ibarra M R, De Teresa J M, Algarabel P A, Marquina C, Blasco J, Garcia J, Oseroff S and Cheong S W 1997 *Phys. Rev.* B **56** 8902
[12] Schiffer P, Ramirez A P, Bao W and Cheong S W 1995 *Phys. Rev. Lett.* **75** 3336
[13] Goodenough J B 1955 *Phys. Rev.* **100** 564
[14] Sehlin S R, Anderson H U and Sparlin D M 1995 *Phys. Rev.* B **52** 11 681
[15] Ramakrishnan T V 1998 *Phil. Trans. R. Soc.* A **356** 5
[16] Hundley M F and Neumeier J J 1997 *Phys. Rev.* B **55** 11 511